**Atmospheric
Chemistry
and Physics
Discussions**

Evolution of anthropogenic pollution at the top of the regional mixed layer in the central Mexico plateau

**D. Baumgardner[1], M. Grutter[1], J. Allan[2], C. Ochoa[1], B. Rappenglueck[3],
L. M. Russell[4], and P. Arnott[5]**

[1]Centro de Ciencias de la Atmósfera, Universidad Nacional Autónoma de México,
Mexico City, Mexico
[2]School of Earth, Atmospheric & Environmental Science, University of Manchester,
Manchester, UK
[3]Earth and Atmospheric Sciences Dept., University of Houston, Houston, TX, USA
[4]Scripps Institution of Oceanography, University of California San Diego, La Jolla, CA, USA
[5]Dept. of Physics, University of Nevada, Reno, NV, USA

Title Page

Abstract	Introduction
Conclusions	References
Tables	Figures

|◄ | ►|

◄ | ►

Back | Close

Full Screen / Esc

Printer-friendly Version

Interactive Discussion

Abstract

The concentrations of gases and properties of aerosol particles have been measured at the mountain site of Altzomoni approximately equidistant from Mexico City, Puebla and Cuernavaca, at an altitude of 4010 m. At this location there is a diurnal transition from local to regional mixed layer air whose properties depend on prevailing winds and larger scale circulation. Three days during March 2006 have been evaluated during which time the synoptic scale air flow was from the east, southeast and southwest. In general the properties of gases and particles were similar when the regional mixed layer (RML) was below the research site, regardless of the direction of flow. When the RML reached the site, the highest concentrations of CO, O_3 and aerosol particles were from the east, decreasing as the flow shifted to the southeast then to the southwest. The maximum concentration of condensation nuclei (CN) was greater than 25×10^{-3} when winds were from the east. The highest mass concentrations of organic matter (OM), sulfate (SO_4^-), and Nitrate (NO_3^+) were 80, 4 and 8 $\mu g\,m^{-3}$, at standard temperature and pressure in air from the east. The mass concentration of OM in the RML was greater than 70% of the total mass, regardless of the air mass origin. This compares to less than the 60% that has been reported for Mexico City.

At night, the mass fraction of sulfate went up by a factor of ten from the daytime value when air arrived from the east. The relationship between the CO and OM suggests that the majority of the daytime OM is from biomass burning and at night it is from wood burning.

Whereas the maximum CO at Altzomoni, 0.35 ppm, was approximately one tenth of the CO measured at the same time in the center of Mexico City, the maximum O_3 of 120 ppb was approximately the same as in the city. The maximum nighttime values of O_3 was 60 ppb, indicating the presence of residual pollution.

From these results we conclude that even though Mexico City is the second most populated city in the world, with an associated high level of pollution, there are other significant sources of pollution in Mexico that contribute to the mixture of emissions

that are dispersed throughout the region. This mixture rapidly erases the signature of a unique Mexico City "plume" and suggests that the environmental impact of this region should be considered as one that stems from a large area source rather than a single megacity.

1 Background

Many papers have addressed the issues of the regional and global impact of anthropogenic emissions from Mexico City, a large urban area classified as a megacity due to its population of greater than 18 million people. Since the early 1990s there have been several major field programs that focused on characterizing the pollution produced by this city and evaluating its impact on health and climate. The first of these programs, Project Aguila, was the only one to study the vertical structure of pollution in Mexico City prior to 2006. This program deployed the NSF/NCAR King Air for two weeks in February of 1991 (Nickerson et al., 1992, 1993; Perez and Raga, 1998) and, in addition to revealing the large variation in gas and particle concentrations over different parts of the city, it was the first time that the vertical profiles of particles and gases were directly measured. As shown in Fig. 1, there were elevated layers of ozone (O_3) and condensation nuclei (CN) that were detected in the morning sounding at 11:00 LST during this flight on 13 February 1991. These were daily features that were verified on other days. The maximum in O_3 at the top of the mixed layer was subsequently simulated by Raga and Raga (2000) who showed that it was the light absorbing layer of aerosols at the top of the mixed layer that led to a decrease in actinic flux and hence a higher photochemical production rate of ozone at the top than at the bottom of the layer. Elevated layers of aerosols also lead to local heating that further stabilizes the mixed layer (Raga et al., 2000), increasing the concentration of aerosols that further enhance photochemical reactions (Dickerson et al., 1997).

Figure 1 also illustrates that although Mexico City is at an altitude of 2270 m, and is surrounded by mountains on the east, south and west, the particles and gases that

Pollution in the regional mixed layer of central Mexico

D. Baumgardner et al.

rise with the growth of the mixed layer can reach elevations as high as the mountain passes, whose altitudes are marked on this figure.

In 1997 another major field campaign, the Investigacion sobre Materia Particulada y Deterioro Atmosferico – Aerosol and Visibility Research (IMADA-AVER) was con-
5 ducted in February and March (Edgerton et al., 1999). During that project measurements were made with wind profilers that provided further evidence that the Mexico City mixed layer grows as much as 3000 m above the basin of the city (Whiteman, 2000).

The vertical structure of the atmosphere measured by aircraft and wind profilers suggests that the city's pollution will rise to levels where prevailing winds then transport
10 it regionally. Indeed, various modeling studies that followed the 1997 field program simulated the transport of particles out of the Mexico City basin (Fast et al., 1998; Whiteman et al., 2000); however, until recently there have been no measurements that could quantify the magnitude of anthropogenic pollution that was transported through any of the mountain passes around the city.

15 In late 2005 a research site was established on the Altzomoni ridge that is located in the Pass of Cortez between the volcanoes of Popocatepetl and Iztaccíhuatl that rise to the southeast of Mexico City. This site was selected because of its altitude of 4010 m and its location in one of the mountain passes where the previous modeling studies (Fast et al., 1998; Whiteman et al., 2000) indicated that air masses from Mexico City
20 would eventually arrive by midday. Preliminary measurements of carbon monoxide (CO), O_3 and other gases had also been made near this location in late April and early May of 1999 using a van provided by the Mexico City government (Jimenez, 2004). Figure 2 is an example of CO and O_3 measured during three days in that period compared to measurements made on the same days at Merced, a site in the
25 center of the city, also operated by the city government as part of its Red Automática de Monitoreo Atmosférico (RAMA). The daily frequencies are the same but shifted in phase as would be expected if the mixed layer grows and is transported from the city. These measurements motivated a more detailed investigation whose measurements are presented in the following evaluation of the properties of gases and particles that

Pollution in the regional mixed layer of central Mexico

D. Baumgardner et al.

were sampled during an intensive operation period (IOP) in March 2006.

2 Instrumentation

The suite of instruments that was operated during the IOP consisted of sensors for establishing the meteorological state of the atmosphere, the concentration of the principal trace gases and analyzers for determining the physical, optical and chemical properties of aerosol particles. The complete list of instrumentation is listed in Table 1 along with the associated parameter that was measured, the responsible institute and their sensitivity and accuracy.

The state parameters, winds and the solar and UV radiation were recorded once per minute from the weather station[1] that was located at an altitude of two meters AGL. Measurements of CO and O_3 were made with an active Fourier Transform Infrared (FTIR) spectrometer, operated with a path length of 350 m. The spectra from this remote sensing system, acquired at a rate of 1 Hz and $0.5\,cm^{-1}$ resolution, were averaged to a sample interval of every five minutes. The concentration of Peroxiacetil-nitratos (PANs) were made with a dual column gas chromatograph[2] equipped with an electron capture detector.

The concentration of particles larger than approximately 10 nm was measured with a TSI [3] model 3010 that was part of the TSI scanning mobility particle sizer (SMPS) that also provided size distributions from 20 to 514 nm. The upper threshold was limited due to the restriction on high voltage when operating at elevated altitudes where corona discharge occurs if a voltage of 5000 V is exceeded. Size distributions for particles larger than 300 nm were measured with the LasAir Model 310[4] that optically sized

---

[1]Davis Instruments

[2]Metcon Inc., Königstein, Germany

[3]Thermal Systems Incorporated, St. Paul, MN

[4]Particle Measuring Systems, Boulder, CO

Pollution in the regional mixed layer of central Mexico

D. Baumgardner et al.

Title Page

Abstract | Introduction

Conclusions | References

Tables | Figures

|◄ | ►|

◄ | ►

Back | Close

Full Screen / Esc

Printer-friendly Version

Interactive Discussion

particles from 0.3 to 25 μm.

The absorption and scattering coefficients were measured with two systems, a Particle Soot Absorption Photometer (PSAP)[5] and a Nephelometer[5], both operating at a wavelength of 550 nm and a Photoacoustic Soot Spectrometer (PASS)[6] that used a laser with a wavelength of 850 nm. The chemical properties were measured with an Aerodyne Aerosol Mass Spectrometer[7] (Canagaratna et al., 2007). Particle data were acquired with several different data systems before merging after time synchronization and averaging to a common time base of a sample every fifteen minutes for the analysis presented in this study.

Sub-micron filter samples were taken every 12 h and Fourier Transform Infrared Spectroscopy (FTIR) was used to quantify particulate organic functional groups, including saturated aliphatic (alkane), unsaturated aliphatic (alkene), aromatic, alcohol, carbonyl, amines, and organosulfate compounds (Maria et al., 2002, 2003; Gilardoni et al., 2007).

All of the instruments were housed in a lightly insulated utility shed with no environmental controls of temperature or humidity. All the particle instruments, with the exception of the LasAir, sampled aerosols from a $PM_{1.0}$ cyclone separator[8]. The sample line from the cyclone to the nephelometer, PSAP and CN counter was heated to approximately 40°C to maintain the particles at low humidity. The purpose of the cyclone was to minimize truncation errors in the measurement of the scattering coefficient with the nephelometer and the aerosols were dried to prevent humidity enhancement of the absorption coefficient measured by the filter-based PSAP. The LasAir was operated in front of the cyclone in order to sample the coarse mode particles. The nephelometer was calibrated in accordance with the recommendations of the manufacturer, corrections were applied to the measurements of the PSAP to account for scattering effects

---

[5]Radiance Research, Seattle, Wa

[6]Droplet Measurement Technologies, Boulder, CO

[7]Aerodyne Inc., Billerica, Ma

[8]University Research Glassware, Chapel Hill, N.C

(Bond et al., 1999) and the aerosol mass spectrometer was calibrated twice during the project while installed at the research site.

3 Results

3.1 Measurement site

As shown in Fig. 3, Altzomoni (19.117° N, 98.654° W, 4010 m a.s.l.) is located approximately equidistance southeast of the center of Mexico City, northeast of Cuernavaca and east of Puebla. During the month of March, a number of different large scale circulation patterns evolved (Fast et al., 2007) during which time the air that arrived at Altzomoni came from nearly all quadrants. Three days have been selected for the current evaluation based upon the analysis of back trajectories produced by the NOAA HYSPLIT program and using the final analysis (FNL) of the Global Forecasting System for the 650 mb level (the average pressure at Altzomoni was 630±5 mb). The days selected were 16, 18 and 19 March, during which times the air mass trajectories were from the east, southeast and southwest, respectively, during daytime and night time. These days were selected as those with no influence from local biomass burning or heavy clouds and precipitation. The yellow lines in Fig. 3 show the 24 h trajectories for the three days where the end times of the trajectories was 14:00 (all times will hereafter be reported in local standard time). It should be noted that the 500 mb winds for these days (Fast et al., 2007) were from south (16 March) and southwest (18 and 19 March).

The measurement site was situated at the highest point on the ridge with an unobstructed view in all directions (Fig. 4). As seen in Fig. 5, the terrain slopes toward the west more abruptly than the east, a feature that will be discussed in greater detail in Sect. 4.0 as it relates to the differences between air masses of different origins. In addition to its strategic location with respect to nearby urban areas, there are no significant local sources of contaminants since it is situated in the national park of Izta-Popo-Zoquiapan with only a single road nearby that is principally used to bring

weekend tourists to the park center that is approximately five km to the southeast of the research site. The days selected for the current study were those where the RML was clearly observed to grow to above the measurement site, as illustrated in Fig. 6, and whose daily trends in gas and particle concentrations exhibited a sharp gradient, as will be shown in the analysis below. The photos shown in Fig. 6 were taken with a web camera looking westwards whose images were recorded every five min during daylight hours throughout the project.

In the following analysis, the measurements are grouped according to the direction of the 24 h trajectories and the results are shown as diurnal averages for the three cases, where each data point is a fifteen minute average. Hence, in each of the figures with time series, the blue, black and red curves are for the days when air was arriving from the east, southeast and southwest, respectively.

3.2 Meteorology

The general meteorological conditions for the March 2006 period have been discussed in detail by Fast et al. (2007), the month when the Megacities Initiative: Local And Global Research Observations (MILAGRO) international field campaign (Molina et al., 2008) was being conducted. Figure 7 shows the daily averages of temperature, relative humidity (RH), and the local wind speed and direction for the three cases. The air masses from the east are generally a couple of degrees warmer in the morning hours (Fig. 7a). The temperature in the southwesterly flow eventually increases until it is the same as in the easterly flow by 08:00 LST. Note that there is no meteorological data on days with air from the southwest between 10:00 and 17:00 due to a problem with downloading data during that time period.

In the early morning hours the relative humidity (RH) of air from the southwest (Fig. 7b) was five time as high as easterly and southeasterly air, but all of the cases showed that the air dried to a minimum of 10% humidity between 06:00 and 10:00 before increasing again throughout the afternoon. The southeasterly and southwesterly humidity increased to a maximum humidity of approximately 80% whereas the RH in

the easterly flow remained low until 18:00 when the winds fell to almost zero and the RH increased to a constant value of 50% throughout the remainder of the evening.

The wind velocities varied widely throughout the day (Fig. 7c). The southwesterly flow had the weakest winds that varied between 2–4 ms^{-1}. The winds from the eastern sector were much stronger, varying between 2–14 ms^{-1}. The winds in the easterly and southeasterly flows remained strong from midnight until 13:00 when they decreased to their minimum values between 18:00 and 20:00.

As shown in Fig. 7d, although the larger scale flow comes from the east, southeast and southwest, the local winds remains nearly constant at 135° in the easterly and southeasterly flow and between 180° and 225° in the southwesterly flow. After 14:00, when the wind velocity was nearly zero, the wind directions have no meaning.

3.3 Gas concentrations

The daily averages of CO, O$_3$ and Peroxyacetyl nitrate (PAN) are shown in Fig. 8a–c, along with the ratio of peroxypropionyl nitrate (PPN) to PAN (Fig. 8d). The CO at Altzomoni remains at its minimum of 0.10 ppm, regardless of air mass origin, from midnight to 10:00. The CO in the air mass from the east and southwest begins to increase at that time. In the southwest air mass the CO gradually increases throughout the afternoon and evening, reaching its maximum concentration of 0.15 ppm at 18:00. The concentration of CO in the easterly air flow increases rapidly before reaching the first maximum of 0.30 ppm at 13:30 and another maximum of 0.35 ppm at 15:00. It then decreases to a minimum of 0.10 ppm at 17:30 before abruptly increasing to a concentration of 0.28 ppm at 18:00 after which time it decreases to a constant value of 0.20 ppm at 20:00 and remains there throughout the evening. The increase in concentration at 18:00 is associated with the period of very low wind velocity. The southeasterly flow maintains the minimum value of 0.10 ppm until 14:00 at which time it reaches its maximum value of 0.20 ppm in a one hour period and remain at this concentration until 20:00 when it begins.

The O$_3$ in the flow from the east and southeast is correlated with the CO showing the

Title Page

Abstract | Introduction

Conclusions | References

Tables | Figures

◄ | ►|

◄ | ►

Back | Close

Full Screen / Esc

Printer-friendly Version

Interactive Discussion

same times for peaks. The maximum in the O_3 concentration from the east is 120 ppb and 80 ppb in air from the southeast. The O_3 from the southwest has a different trend than the CO, increasing from a minimum of 40 ppb at 08:00, reaching a maximum of 70 ppb at 15:00 before decreasing back to a minimum value at 22:00. The night time concentrations of O_3 in the easterly and southeasterly flow are between 60 and 80 ppb, compared to night time, minimum values of 20 ppb measured in Mexico City at the same time at the Merced air quality monitoring station operated as part of the RAMA network.

The PAN (Fig. 8c) is below the detection limit until 11:00, regardless of the direction of flow. In the southwest flow the PAN concentration, although less than 1.0 ppb, has the same trend as CO during that period. The PAN in the flow from the east doesn't exceed the detection level until 13:30 at which time it increases to a maximum near 4.0 ppb before decreasing again below detection levels at 16:00. It does not reflect the first maximum at 13:30 that was seen in the CO for this day. The PAN from the southeast has a trend similar to the CO and reaches its maximum of 0.5 ppb at 15:00.

Given that PPN is primarily a result of fresh, anthropogenic emissions (Gaffney, 1998) the ratio of PPN to PAN (Fig. 8d) shows that only the PAN in the flow from the eastern sector has anthropogenic influence.

3.4 Particle properties

The daily trends in the particle number and mass concentrations are plotted in Fig. 9, normalized to standard temperature and pressure (273.16°C, 1023.25 mb) to facilitate easier comparison with measurements made at other altitudes and locations during MILAGRO. The number and mass concentrations generally follow the trends in CO, regardless of the air flow direction, showing the same times for maxima in number and mass. The maximum in CN of greater than 25×10^{-3} in the airflow from the east is almost twice the maxima from the southeast and southwest, both of about 15×10^{-3}. It is worthy to note that the average daily maximum measured with the same instrument in Mexico City in April 2005 was 30×10^{-3} (Baumgardner et al., 2007).

Compared to the CN measurements that are dominated by the particles less than 0.1 μm, the measurements from the LASAir optical particle counter (OPC) are of particles >0.3 μm, which include part of the accumulation mode and most of the coarse mode particles. The OPC concentrations (Fig. 9b) mirror those of CN and are quite high, exceeding 1000 cm^{-3} in the easterly flow. The behavior of particles larger than 0.3 μm is magnified when the number concentrations are converted to mass concentrations. The mass concentrations in particles less than 1.0 μm and 10 μm, also known as PM$_{1.0}$ and PM$_{10}$, were derived from the size distributions of the number concentrations measured with the OPC. These number distributions were converted to volume distributions assuming spherical particles, then multiplied by an average particle density of 1.9 g cm^{-3} estimated from the relative mass fraction of ions measured by the AMS and from black carbon (BC) derived from the PSAP, following the equation of DeCarlo et al. (2004). The trends in PM$_{1.0}$ and PM$_{10}$ are shown in Fig. 9c and d. As expected, the mass concentrations follow a similar pattern to the OPC number concentration with the exception of the PM$_{10}$ in the flow from the east that has a very large peak at 11:30. Given that this peak is not reflected in the CN or PM$_{1.0}$ these large mass concentrations are likely a result of dust from a local source. The area immediately east of the research site is largely devoid of trees and consists of small scrub brush and dry soil; hence, the particles larger than a few micrometers are probably locally generated dust.

The ion mass concentrations and effective black carbon (EBC), also normalized to standard temperature and pressure, are displayed in Fig. 10. The EBC is not a true measure of the BC because it is derived from the absorption coefficient measured with the PSAP by using a specific absorption coefficient, ω_a, of 10 m^2 g^{-1} to convert to BC mass. As discussed in detail by Bond and Bergstrom (2006), ω_a can vary widely depending on the properties of the BC. The value used in the present study is taken from the literature as being the most common, but with the caveat that the numbers presented here have at least an uncertainty of ±50%. A second caveat is that during the morning of flow from the southwest, the data is missing from the AMS between 01:00 to 10:30 due to a problem with the data system.

The mass concentration of organic matter (OM), shown in Fig. 10a, is the largest in air coming from the east. The maximum OM concentration is almost $80\,\mu g\,m^{-3}$ compared to $20\,\mu g\,m^{3}$ from the southeast and $10\,\mu g\,m^{-3}$ in air from the southwest. The OM in the easterly flow has multiple peaks during the day, similar to those seen in the CN but not always at the same time. The concentration increase in OM starts earlier from the southwest then reaches a constant value at 11:00, never changing throughout the remainder of the day and evening. The OM in the southeasterly flow increases later than in the easterly flow then decreases very slowly throughout the day, reaching the minimum value by midnight.

The sulfate ion mass concentration, SO_4^{-}, seen in Fig. 10b, has distinctly different patterns depending on the origin of the air mass. In the easterly flow, sulfate does not start increasing until after 13:00, unlike the OM that abruptly increased at 12:00. After reaching a peak value of $3.0\,\mu g\,m^{-3}$, its follows a trend similar to the CO where the concentration decreases until 17:30 before rapidly increasing to an even higher maximum of $3.9\,\mu g\,m^{-3}$ at 18:00. In the southwest flow, the sulfate is much lower in concentration and also tracks the changes in CO. The maximum value is $2.0\,\mu g\,m^{-3}$. The sulfate in the southeasterly flow varies between 1.0 and $2.5\,\mu g\,m^{-3}$ during the morning hours from midnight until 08:00 when it decreases to a minimum at midday before increasing once again to a concentration of $2.5\,\mu g\,m^{-3}$ where it remained until 23:30.

As shown in Fig. 10c and d, the ion mass concentrations of nitrate, NO_3^{+}, and ammonium, NH_4^{-}, have nearly identical trends that match those of the SO_4^{-} concentrations in the flows from all directions.

The EBC (Fig. 10e) shows trends in the easterly and southeasterly flows similar to the nitrate but the EBC in the southwesterly flow is not correlated with any of the other gas or particle concentrations. The maximum concentration of EBC is from the east with a value of over $1000\,ng\,m^{-3}$, twice the concentration in the southeasterly flow and three times that of the EBC in the air from the southwest.

"The FTIR analysis was separated into periods when the filters were exposed in the

daytime when the site was in the RML, 11:00–18:00, and then above the RML at night and early morning, 18:00–11:00 (following day), for the days when winds were from the east and southwest. The daytime proportion of the alcohol and alkane groups, 53% and 17%, respectively, were the same regardless of flow direction. The amines were higher from the east, 26% vs. 15% and carboxylic acids were a larger percentage from the southwest, 14% vs. 5%. The principal difference in the organic composition between the easterly and southwesterly air masses is in the alcohol and alkane groups at night. The alcohol group dominates the organics making up 69% in the easterly flow while alkanes make up 45% of the organics in the southwesterly flow. Carboxylic acids in the southwesterly flow make up another 30% of the organics compared to only 7% in the easterly flow.

The daily trends in the absorption, scattering and extinction coefficients and the single scattering albedo are displayed in Fig. 14a–d. The absorption coefficient, B_{abs}, matches the pattern in EBC, previously described, since the EBC was derived directly from B_{abs}. The scattering coefficient, B_{sct}, reflects the trends in the OM for all air flow directions.

4 Discussion

The daily trends in gas and particle concentrations are consistent with a meteorological pattern in which the morning boundary layer in the regions below Altzomoni begins to increase in depth by turbulent mixing as the surface is heated by solar radiation and larger scale eddies are generated by the vertical wind shear. As described by Fast et al. (1998) and Whiteman et al. (2000) the dynamics in the region of Mexico City are complex but on average, during the March time frame, flow up the sides of the mountains develops due to the thermal gradient produced by solar heating of both sides of the surrounding mountains. As the depth of the RML increases the larger scale flow will transport the gases and particles in the upper part of the layer away from the primary sources. Boundary layer growth is a result of entrainment and mixing

of free tropospheric air at the top of the boundary layer. In the absence of any new sources, the primary gases and particles will be diluted as they are transported and dispersed.

In 2006, the RML, as measured by wind profilers, radiosondes and lidar (Shaw et al., 2007) grew to an average depth of 3000±1000 m AGL by 17:00 LST±1 h. Based on these measurements, made at several locations 30–50 km to the northeast of Mexico City, the RML would reach the height of 1700 m, the relative height of Altzomoni above the Mexico City basin, at 12:00±1 h. The concentration of gases and particles at Altzomoni will begin to increase as the RML reaches the site, mixing with the local environment and achieving a maximum value as the top of the RML, where entrainment and mixing is most vigorous, continues to ascend above the ridge. After this time the concentrations will either decrease as dilution with free tropospheric air continues or, depending on the strength of the source and the local dynamics, the concentrations will remain approximately constant until the source of turbulent mixing is removed. By late afternoon, as the solar heating decreases, the surface begins to cool and the thermal structure boundary layer become more stable, cutting off the principle source of energy and initiating the decrease in the mixed level depth. In the region of Altzomoni the cooling of the mountain slopes produces a gradient flow down the hill sides with a subsequent decoupling between some fraction of the air in the upper portion of the RML and the air below. This forms an elevated, residual layer with higher concentrations of pollutants that remains after the lower of RML has receded below the altitude of the research site.

The CO and particle concentrations (Figs. 8 and 9) in the easterly and southwesterly flows show the first indication RML air between 10:00 and 11:00. The southwesterly flow reaches its peak concentrations first at 12:00, followed by the easterly at 13:30 then southeasterly flow at 15:00. The differences in time when the concentration maxima are reached is a function of the local topography and the strength of the flow. As Fig. 5 shows, the western slope of the ridge is much steeper so that when flows are from the west the RML air will rise more rapidly. In addition, the sources of anthro-

pogenic emission are closer to Altzomoni on the west side than on the east where the change in altitude is much more gradual.

The interaction of topography and dynamics can also lead to oscillations in the depth of the RML so that the top of this layer can move up and down during the day. This is the likely source of the decrease then increase in the concentrations during the day when the flow is from the east as the RML first grows above the Altzomoni site at 14:00, recedes as the wind speed decreases then moves above the site as the flow increases again from the east. On the days with flows from the southeast and south west, the gas and particle concentrations remain approximately constant as the rate of dilution by mixing and entrainment is balanced by a constant flow of new material arriving from the sources of pollution. This continues until cooling of the surface begins late in the afternoon around 20:00 and the RML recedes, leaving behind a part of the contaminated air in the residual layer.

Measurements in 1997 in the southwestern sector of Mexico City (Raga et al., 1999), at a hillside research site 440 m above the city, showed concentrations of approximately 40 ppb in ozone at night time compared to values less than 20 ppb in the city. The higher values in O_3 were a result of the residual layer that remained after the nocturnal boundary layer had formed. At Altzomoni we see a similar trend except the residual layer O_3 is much higher in concentration, between 60 and 80 ppb.

It is instructive to compare a number of parameters measured at Altzomoni with similar variables measured at other locations during the same or previous time periods. Several aircraft were operated during MILAGRO (Molina et al., 2008) and two of them, The Department of Energy (DOE) Gulfstream-1 and the NCAR/NSF C-130 carried aerosol mass spectrometers and CO analyzers, as well as many other gas and particle analyzers. The C130 made two vertical profiles approximately 50 km to the east of the Altzomoni research site on 29 March (DeCarlo et al., 2008). The average values of OM and sulfate at 4000 m were approximately 5 and 4 μg m^{-3}, respectively, normalized to standard temperature and pressure (STP). As seen in Fig. 10, the average maximum OM and sulfate concentrations range from 10–80 μg m^{-3} and 1–4 μg m^{-3}, respectively.

Hence the aircraft was measuring similar sulfate but lower OM than at the ground site, although the OM values are similar when comparing the aircraft data with early morning and late afternoon and evening periods at Altzomoni.

Measurements were made with an Aerodyne AMS in Mexico City during the 2003 MCCMA campaign (Molina et al., 2007; Salceda et al., 2006) and it was found that, on average, the OM, sulfate, nitrate and EBC contributed 59%, 11%, 11% and 12%, respectively to the $PM_{2.5}$ mass, when removing the contribution from soil. At Altzomoni, as seen in Fig. 13, relative contributions of the ions and EBC depended on where the RML was in relation to the research site and the direction of the air flow. Regardless of the flow direction, in or out of the RML, the OM was the largest contributor to the total mass. In the daytime it was 81%, 70% and 69% of the mass of particles coming from the east, southeast and southwest. At night these proportions changed to 54%, 48% and 65%. There was almost no change in how mass was apportioned between night and day in the southwesterly flow; however, in the easterly and southeasterly flow, the fraction of sulfate was three to ten times larger at night, depending on whether flow was from the southeast or east.

The diurnal trends in the mass fractions are shown in Fig. 14. Because of the problem with the AMS in the morning hours on the day with southwesterly flow, we can only discuss the full cycle in mass fractions of OM and sulfate during the easterly and southeasterly flow. These mass fractions are negatively correlated as the sulfate mass fraction is maximum at night and minimum during the day whereas the OM follows the reverse trend. The mass fraction of EBC is largest in the morning in the easterly flow while generally small in the northeasterly flow except for a gradual increase in the fraction of mass it contributes until the RML arrives and the total mass becomes dominated by the OM.

Measurements of OM from aircraft during MILGRO were normalized with CO to account for the effect of dilution as the RML grows and is transported from the primary source of the CO (Kleinman et al., 2007; DeCarlo et al., 2008). The values of OM/CO in these aircraft measurements varied between about 10 and 80 and reflected changes

in the age of the air where high values are related to locations further from the source (Kleinman et al., 2007). In Fig. 15, the daily trends in OM/CO, SO_4/CO, NO_3/CO and EBC/CO show that morning and nighttime ratios are much smaller than periods in the afternoon when the RML is present. Given that CO is a conservative tracer the higher ratios in the RML at Altzomoni indicate, in part, secondary production of OM and SO_4. The range in OM/CO in southeasterly and southwesterly flow is similar to the aircraft measurements; however, the low OM/CO values are not a result of being close to the primary emissions as was the case with the aircraft, but are background values in air that has been transported from much further away. The maximum OM/CO, SO_4/CO and NO_3/CO values are very similar to those measured by Kleinman et al. (2007) in air they identified with aging less than 12 h.

The mass concentrations of OM and inorganic compounds do not show a significant decrease in concentration as related to the possible origins of the air masses. Average maximum values of CO in Mexico City during the March 2006 period ranged from 3–5 ppm, as measured at the RAMA station at Merced whereas the maximum CO at the Altzomoni site was between 0.20 and 0.35 ppb, or approximately a factor of ten dilution. The maximum CN concentrations at Altzomoni were between 15 000 and 30 000 cm^{-3}, only a factor of 2–3 lower than similar measurements made in the city (Baumgardner et al., 2007). Salcedo et al. (2006) report average concentrations of OM and sulfate of 21 and 3 $\mu g\,m^{-3}$. At Altzomoni the mass concentrations are between 1–80 and 0.2 and 4.0 $\mu g\,m^{-3}$, respectively. In addition, the O_3 concentration maxima at Altzomoni between 80 and 120 ppb are similar to the daily maxima in Mexico City. From this we conclude that O_3 and particles at the Altzomoni site are not only coming from the primary emissions, but there are additional sources that offset the dilution as the RML grows.

As discussed by Maria et al. (2003) the relationship between CO and OM is an indicator of organic aerosol source types and secondary organic aerosol formation. Sulfate, ammonium, and nitrate, as seen in the diurnal trends (Fig. 10) are also associated with many of these same combustion sources, so that the CO/OM slope is also

a source indicator for inorganic species.

Figure 16 is a plot of CO versus OM for the three days, where each of the points is a fifteen minute average. The color of the symbol indicates the hour of the day as given by the scale to the right in the figure. The three lines, numbered 1–3 are CO/OM relationships that have been established for primary sources of emissions: (1) diesel trucks (Lloyd and Cackette, 2001), (2) wood burning (Cabada et al., 2002) and (3) biomass burning (Andreae and Merlet, 2001). Note that the relationships 1–3 shown in this figure were derived for CO versus organic carbon (OC) rather than for OM that is measured by the AMS. These lines have been adjusted by a factor of 1.8 according to the average relationship between OM and OC that has been established by Takegawa et al. (2005).

The day time pairs of CO and OM fall close to the line indicating biomass burning whereas at night most of the points are closest to the relationship that indicates wood burning. This suggests that in addition to those pollutants produced by the major urban areas, there is also a significant contribution from biomass burning. The days that were selected for this study were those where visual observations showed no obvious fires burning in the surrounding area, such as those that were evident in the first quarter of March. As reported by Yokelson et al. (2007), however, satellite observations show 218 fires in the study area and there was wide spread burning of waste in the Yucatan peninsula to the southwest. The air flow direction does not change the CO to OM slopes. There are large agricultural areas in the Puebla valley and to the south of the mountains are other large agricultural areas where burn-off of planting areas in the spring is a routine practice. The larger concentrations in flow from the east probably reflects the closer proximity of wood fires and biomass burns while the lower concentrations from the southeast are from the more diluted emissions from the Yucatan. As discussed by Yokelson et al. (2007) ammonium is another reactive fire emission that could contribute to aerosol particles such as ammonium sulfate or ammonium bisulfate and affect secondary aerosol formation in general. As seen in Fig. 10b and d, there was a large amount of sulfate and ammonium at night time in the southeasterly

flow and the sulfate was 30% of the total mass at night in the flow from the east and southeast, indicating secondary formation of sulfate compounds.

Another indicator of the source of anthropogenic pollution and the relative mix of fuel types during the combustion that produces the majority of primary particles and gases is the slope of the BC to CO relationship (Baumgardner et al., 2001). As shown in Fig. 17, when compared with the BC to CO relationship measured in Mexico City in 2005 (Baumgardner et al., 2007), the day time relationship between BC (EBC in this study) and CO fall in three groups: early to mid-morning, afternoon and nighttime. Before the RML arrives in the early to mid-morning, the EBC to CO relationship has the steepest slopes and at night the slope is closer to the relationship measured in Mexico City. When the slope is steep, these are periods also when the CO to OM comparison indicated wood or biomass burning. When the RML arrives at Altzomoni, the CO increases with respect to the EBC and then at night a residual layer of CO remains while the concentration of BC particles decrease by deposition and coagulation.

5   Summary and conclusions

Measurements of gas concentrations and particle properties at a mountain location in the central plateau region of Mexico, at an altitude of 4010 m a.s.l., show that the CO in the regional boundary layer air that arrives at the research site has been diluted by a factor of ten but secondary processes maintain an ozone concentration whose maximum of 110 ppb is similar to that of Mexico City. The CO to OM relationship indicates that biomass and wood burning upwind of the Altzomoni research site produce organic material that is 80% of the total mass. Maximum particle concentrations were greater than 25×10^3 cm^{-3}, only a factor of three less than maxima measured in the center of Mexico City. Large night time concentrations of ammonium and sulfate when flow is from the southeast suggest that emissions from burning in the Yucatan Peninsula are being transported northwards.

From these results we conclude that even though Mexico City is the second most

populated city in the world, with an associated high level of pollution, there are other significant sources of pollution in Mexico that contribute to the mixture of emissions that is dispersed throughout the region. This mixture rapidly erases the signature of a unique Mexico City "plume" and suggests that the environmental impact of this region
5 should be considered as one that stems from a large area source rather than a single megacity.

References

Adachi, K. and Buseck, P. R.: Internally mixed soot, sulfates, and organic matter in aerosol particles from Mexico City, Atmos. Chem. Phys., 8, 6469–6481, 2008,
20 http://www.atmos-chem-phys.net/8/6469/2008/.
Andreae, M. O. and Merlet, P: Emissions of trace gases and aerosols from biomass burning, Global Biogeochem. Cy., 15, 955–966, 2001.
Baumgardner, D., Kok, G. L., and Raga, G. B.: On the diurnal variability of particle properties related to light absorbing carbon in Mexico City, Atmos. Chem. Phys., 7, 2517–2526, 2007,
25 http://www.atmos-chem-phys.net/7/2517/2007/.
Baumgardner, D., Raga, G., Peralta, O., Rosas, I., Castro, T., Kuhlbusch, T., John, A., and Petzold, A.: Diagnosing Black Carbon Trends in Large Urban Areas Using Carbon Monoxide Measurements, J. Geophys. Res.,107(D21), 8342, doi:10.1029/2001JD000626, 2001.

Bond, T. C., Anderson, T. L., and Cambell, D.: Calibration and intercomparison of filter-based measurements of visible light absorption by aerosols, Aerosol Sci. Tech., 30, 582–600, 1999.

Bond, T. C. and Bergstrom, R. W.: Light absorption by carbonaceous particles: An investigative review, Aerosol Sci. Tech., 40, 27–67, 2006.

5 Cabada, J. C., Pandis, S. N., and Robinson, A. L.: Sources of atmospheric carbonaceous particulate matter in Pittsburgh, Pennsylvania, J. Air Waste Manage., 52, 732–741, 2002.

Canagaratna, M. R., Jayne, J. T., Jimenez, J. L. , Allan, J. D. , Alfarra, M. R., Zhang, Q., Onasch, T. B., Drewnick, F., Coe, H., Middlebrook, A., Delia, A., Williams, L. R., Trimborn, A. M., Northway, M. J., DeCarlo, P. F., Kolb, C. E., Davidovits, P., Worsnop, D. R.: Chemical
10 and Microphysical Characterization of Ambient Aerosols with the Aerodyne Aerosol Mass Spectrometer, Mass Spectrom. Rev., 26, 185–222, 2007.

DeCarlo, P. F., Slowik, J. G., Worsnop, D. R., Davidovits, P., and Jimenez, J. L.: Particle Morphology and Density Characterization by Combined Mobility and Aerody-namic Diameter Measurements. Part 1: Theory, Aerosol Sci. Tech., 38, 1185–1205,
15 doi:10.1080/027868290903907, 2004.

DeCarlo, P. F., Dunlea, E. J., Kimmel, J. R., Aiken, A. C., Sueper, D., Crounse, J., Wennberg, P. O., Emmons, L., Shinozuka, Y., Clarke, A., Zhou, J., Tomlinson, J., Collins, D. R., Knapp, D., Weinheimer, A. J., Montzka, D. D., Campos, T., and Jimenez, J. L.: Fast airborne aerosol size and chemistry measurements above Mexico City and Central Mexico during the MILAGRO
20 campaign, Atmos. Chem. Phys., 8, 4027–4048, 2008,
http://www.atmos-chem-phys.net/8/4027/2008/.

Dickerson, R., Kondragunta, S., Stenchikov, G., Civerolo, K., and Doddridge, B: The impact of aerosols on solar UV radiation and photochemical smog, Science, 278, 827–830, 1997.

Edgerton, S. A., Arriaga, J. L., Archuleta, J., Bian, X., Bossert, J. E., Chow, J. C., Coulter, R.
25 L., Doran, J. C., Doskey, P. V., Elliot, S., Fast, J. D., Gaffney, J. S., Guzman, F., Hubbe, J. M., Lee, J. T., Malone, E. L., Marley, N. A., McNair, L. A., Neff, W., Ortiz, E., Petty, R., Ruiz, M., Shaw, W. J., Sosa, G., Vega, E., Watson, J. G., Whiteman, C. D., and Zhong, S: Particulate air pollution in Mexico City: A collaborative research project, JAPCA J. Air Waste Ma. , 49, 1221–1229, 1999.

30 Fast, J. D. and Zhong, S. Y.: Meteorological factors associated with inhomogeneous ozone concentrations within the Mexico City basin, J. Geophys. Res., 103, 18 927–18 946, 1998.

Fast, J. D., de Foy, B., Acevedo Rosas, F., Caetano, E., Carmichael, G., Emmons, L., McKenna, D., Mena, M., Skamarock, W., Tie, X., Coulter, R. L., Barnard, J. C., Wiedinmyer, C., and

Madronich, S.: A meteorological overview of the MILAGRO field campaigns, Atmos. Chem. Phys., 7, 2233–2257, 2007,
http://www.atmos-chem-phys.net/7/2233/2007/.

Gaffney, J. S., Marley, N. A., Cunningham, M. M., and Doskey, P. V.: Measurements of peroxy-
5 actyl nitrates (PANS) in Mexico City: implications for megacity air quality impacts on regional scales, Atmos. Environ., 33, 5003–5012, 1999.

Gilardoni, S., Russell, L. M., Sorooshian, A., Flagan, R. C., Seinfeld, J. H., Bates, T. S., Quinn, P. K., Allan, J. D., Williams, B., Goldstein, A. H., Onasch, T. B., and Worsnop, D. R.: Regional variation of organic functional groups in aerosol particles on four U.S. east coast platforms
10 during the International Consortium for Atmospheric Research on Transport and Transformation 2004 campaign, J. Geophys. Res., 112, D10S27, doi:10.1029/2006JD007737, 2007

Jiménez, J. C., Raga, G., Baumgardner, D., Castro, T., Rosas, I., Baez, A., and Morton, O.: On the composition of airborne particles influenced by emissions of the volcano Popocatepetl in Mexico, Nat. Hazards, 1, 21–37, 2004

15 Kleinman, L. I., Springston, S. R., Daum, P. H., Lee, Y.-N., Nunnermacker, L. J., Senum, G. I., Wang, J., Weinstein-Lloyd, J., Alexander, M. L., Hubbe, J., Ortega, J., Canagaratna, M. R., and Jayne, J.: The time evolution of aerosol composition over the Mexico City plateau, Atmos. Chem. Phys., 8, 1559–1575, 2008,
http://www.atmos-chem-phys.net/8/1559/2008/.

20 Liu, S., Takahama, S., Russell, L. M. , Gilardoni, S., Allan, J., and Baumgardner, D.: Functional Group Signatures of Submicron Organic Aerosols during MILAGRO 2006, Proceedings of the American Association for Aerosol Research, Orlando, FL, October, 2008.

Lloyd, A. C. and Cackette, T. A.: Diesel engines: Environmental impact and control, J. Air Waste Manage. Assoc., 51, 809–847, 2001.

25 Maria, S. F., Russell, L. M., Turpin, B. J., and Porcja, R. J.: FTIR measurements of functional groups and organic mass in aerosol samples over the Caribbean, Atmos. Environ., 36, 5815–5196, 2002.

Maria, S. F., Russell, L. M., Turpin, B. J., Porcja, R. J., Campos, T. L., Weber, R. J. and Huebert, B. J.: Source signatures of carbon monoxide and organic functional groups in Asian
30 Pacific Regional Aerosol Characterization Experiment (ACE-Asia) submicron aerosol types, J. Geophys. Res., 108(D23), 8637, doi:10.1029/2003JD003703, 2003.

Molina, L. T., Kolb, C. E., de Foy, B., Lamb, B. K., Brune, W. H., Jimenez, J. L., Ramos-Villegas, R., Sarmiento, J., Paramo-Figueroa, V. H., Cardenas, B., Gutierrez-Avedoy, V., and

Title Page

Abstract | Introduction

Conclusions | References

Tables | Figures

|◀ | ▶|

◀ | ▶

Back | Close

Full Screen / Esc

Printer-friendly Version

Interactive Discussion

Molina, M. J.: Air quality in North America's most populous city – overview of the MCMA-2003 campaign, Atmos. Chem. Phys., 7, 2447–2473, 2007, http://www.atmos-chem-phys.net/7/2447/2007/.

Molina, L. T., Madronich, S., Gaffney, J., et al.: An Overview of MILAGRO 2006 Campaign: Mexico City Emissions and its Transport and Transformation, Atmos. Chem. Phys., submitted, 2008.

Nickerson, E., Sosa, G., Hochstein, H., McCaslin, P., Luke, W., and Schanot, A.: Project Aguila: in situ measurements of Mexico City air pollution by research aircraft, Atmos. Environ., 26(B), 445–451, 1992.

Nickerson, E., McCaslin, C. P., Sandoval, E., Paramo, V. H., and Gonzalez, E.: Aircraft observations of ozone, carbon monoxide and NO_x over Mexico City during project AGUILA, in: Air Pollution I, editet by: Zanneti, P., Brebia, C. P., Garcia Gardea, J. E., and Ayala Milian, G., Computational Mechanics Publications, Southampton, 793 pp., 1993.

Perez Vidal, H. and Raga, G. B.: On the vertical distribution of pollutants in Mexico City, Atmosfera, 11, 95–108, 1998.

Raga, G. B., Kok, G. L., Baumgardner, D., Rosas, I.: Some aspects of boundary layer evolution in Mexico City, Atmospheric Environ., 33, 5013–5021, 1999.

Raga, G. B and Raga, A. C.: On the formation of an elevated ozone peak in Mexico City, Atmospheric Environ., 34, 4097–4102, 2000.

Raga, G. B., Castro, T., and Baumgardner, D.: The impact of megacity pollution on local climate and implications for the regional environment: Mexico City, Atmos. Environ., 35, 1805-1811, 2001.

Salcedo, D., Onasch, T. B., Dzepina, K., Canagaratna, M. R., Zhang, Q., Huffman, J. A., De-Carlo, P. F., Jayne, J. T., Mortimer, P., Worsnop, D. R., Kolb, C. E., Johnson, K. S., Zuberi, B., Marr, L. C., Volkamer, R., Molina, L. T., Molina, M. J., Cardenas, B., Bernab, R. M., Mrquez, C., Gaffney, J. S., Marley, N. A., Laskin, A., Shutthanandan, V., Xie, Y., Brune, W., Lesher, R., Shirley, T., and Jimenez, J. L.: Characterization of ambient aerosols in Mexico City during the MCMA-2003 campaign with Aerosol Mass Spectrometry: results from the CENICA Supersite, Atmos. Chem. Phys., 6, 925–946, 2006, http://www.atmos-chem-phys.net/6/925/2006/.

Shaw, W. J., Pekour, M. S., Coulter, R. L., Martin, T. J., and Walters, J. T.: The daytime mixing layer observed by radiosonde, profiler, and lidar during MILAGRO, Atmos. Chem. Phys. Discuss., 7, 15025–15065, 2007,

Pollution in the regional mixed layer of central Mexico

D. Baumgardner et al.

Title Page

Abstract	Introduction
Conclusions	References
Tables	Figures

◄ | ►◄

◄ | ►

Back | Close

Full Screen / Esc

Printer-friendly Version

Interactive Discussion

http://www.atmos-chem-phys-discuss.net/7/15025/2007/.

Takegawa, N., Miyazaki, Y., Kondo, Y., Komazaki, Y., Miyakawa, T., Jimenez, J. L., Jayne, J. T., Worsnop, D. R., Allan, J. D., and Weber, R. J.: Characterization of an Aerodyne Aerosol Mass Spectrometer (AMS): Intercomparison with Other Aerosol Instruments, Aerosol Sci. Tech., 39, 760–770, 2005.

Turpin, B. J. and Lim, H. J.: Species Contributions to $PM_{2.5}$ Mass Concentrations: Revisiting Common Assumptions for Estimating Organic Mass, Aerosol Sci. Tech., 35, 602–610, 2001.

Whiteman, C. D., Zhong, S., Bian, X., Fast, J. D., and Doran, J. C.: Boundary layer evolution and regional-scale diurnal circulations over the Mexico Basin and Mexican Plateau, J. Geophys. Res., 105, 10081–10102, 2000.

Yokelson, R. J., Urbanski, S. P., Atlas, E. L., Toohey, D. W., Alvarado, E. C., Crounse, J. D., Wennberg, P. O., Fisher, M. E., Wold, C. E., Campos, T. L., Adachi, K., Buseck, P. R., and Hao, W. M.: Emissions from forest fires near Mexico City, Atmos. Chem. Phys., 7, 5569–5584, 2007,

http://www.atmos-chem-phys.net/7/5569/2007/.

Pollution in the regional mixed layer of central Mexico

D. Baumgardner et al.

Title Page

Abstract | Introduction

Conclusions | References

Tables | Figures

◄ | ►

◄ | ►

Back | Close

Full Screen / Esc

Printer-friendly Version

Interactive Discussion

Table 1. Instrumentation at Altzomoni.

Parameter	Instrument	Institute	Detection Limit	Accuracy
State Parameters Temperature, RH, Pressure	Davis Inc.	UNAM Pressure 100 to 1024	-50 to $+50°$ 0 to 100% ± 1 mb	$\pm$ ± 5%
Winds	Davis Inc.	UNAM	0 to 50 ms^{-1}	
Solar Radiation	Davis Inc.	UNAM	0.285 μm to 2.80 μm 0 to 1400 Wm^{-2}	± 1.5%
UV Radiation	Davis Inc.	UNAM	0.295 μm to 0.385 μm 0 to 60 Wm^{-2}	± 1.5%
CO,O$_3$	Active FTIR	UNAM	1 ppb	± 15%
CN	TSI 3010	UNAM	0.01 μm	± 1.5%
Size Distribution	TSI SMPS 3081	UNAM	0.020–0.514 μm	± 15%
Size Distribution	PMS LasAir 300	UNAM	0.3–25 μm	± 25%
Absorption Coeff.	Radiance PSAP	UNAM	1 Mm^{-1}	± 25%
Absorption Coeff. Scattering Coeff.	DMT PAS Radiance	UNAM UNLV	1 Mm^{-1} 1 Mm^{-1}	± 15% ± 25%
Scattering Coeff.	DMT PAS	UNLV	1 Mm^{-1}	± 15%
SO$_4$, NO$_3$, NH$_4$, OC, Cl	Aerodyne AMS	Scripps/UNAM/U. Manchester	Limit of Detection= 0.1 μg m^{-3}	14%
PAN/PPN	Metcon GC/ECD	U. Houston	50 ppt	± 15%
Visible photography	Web Camera	UNAM	Every 5 min	N.A.
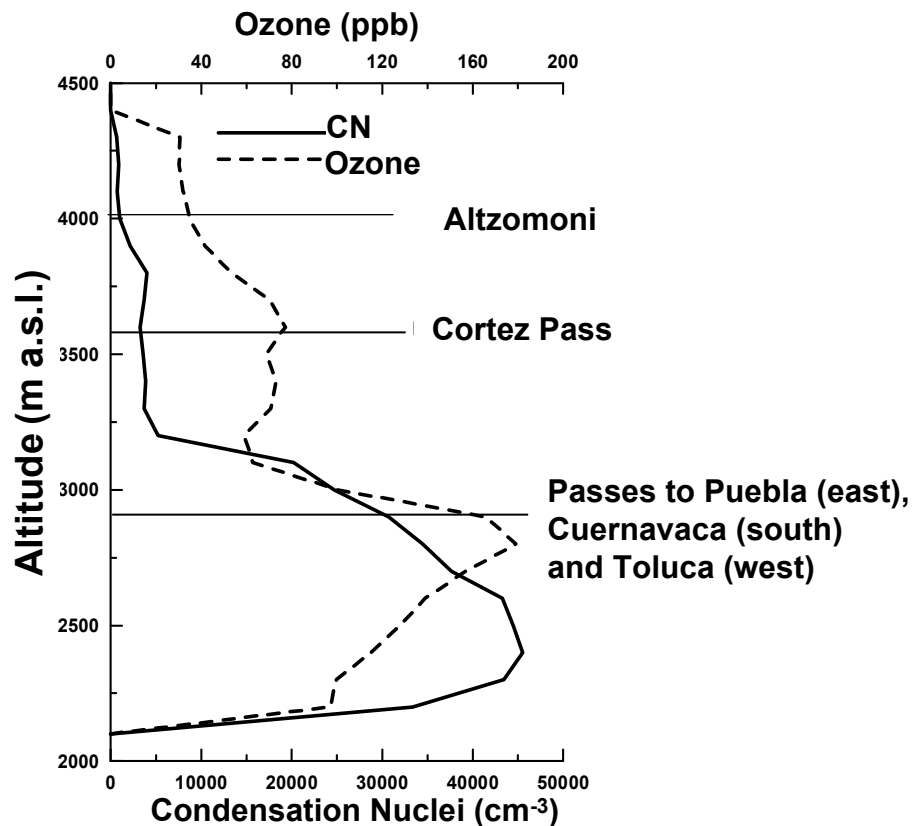
Fig. 1. The concentrations of CN (solid curve) and O_3 (dashed) were measured with the NCAR/NSF King Air on 13 February 1991 during ascents and descents from the Benito Juarez International Airport. The profile in this figure was made at approximately 11:00 LST.
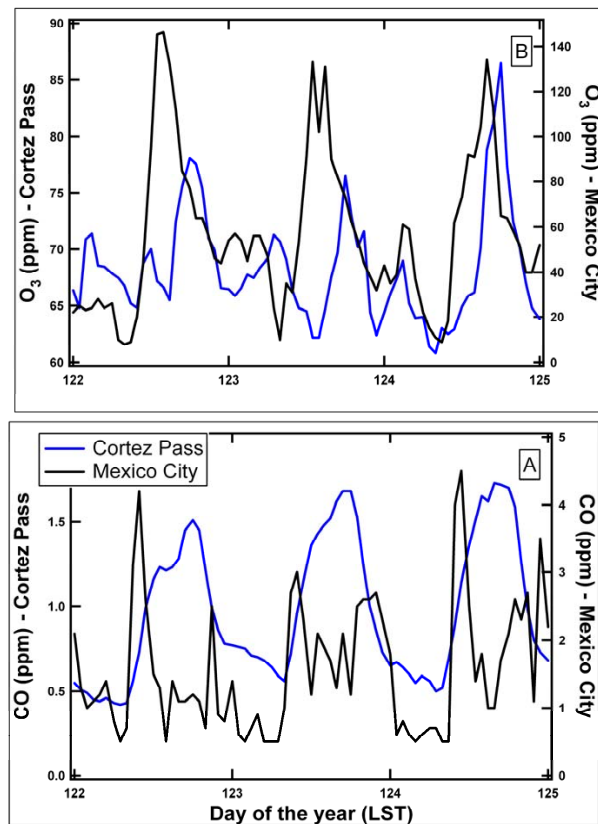
Fig. 2. The time series of **(A)** carbon monoxide and **(B)** Ozone, measured at the Pass of Cortez (blue curve) and in central Mexico City (black curve) in April 1999, show similar daily cycles but several hours out of phase.

Fig. 3. The research site was situated on the Altzomoni ridge in the Pass of Cortez between the Popocatepetl and Iztaccíhuatl volcanoes. Mexico City is approximately 60 km to the northeast, Cuernavaca is 60 km to the southeast and Puebla is 50 km to the east. The yellow lines denote back trajectories for the three days selected for the study presented in this paper.

Full Screen / Esc

Printer-friendly Version

Interactive Discussion
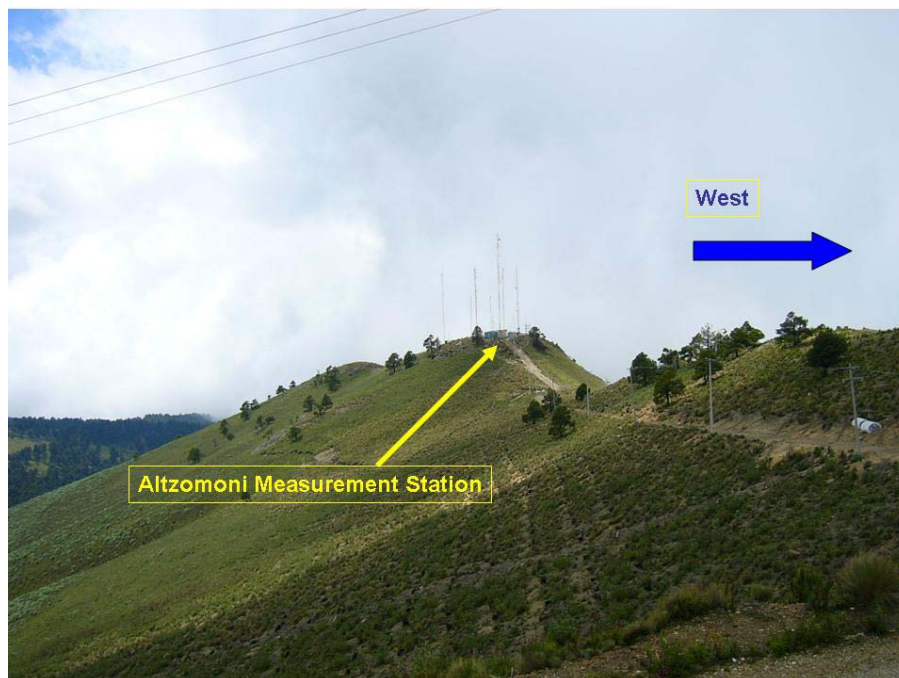
Fig. 4. The research site was at the highest point of the Altzomoni ridge, 4010 m, with an unobstructed, 360˚ view of the region.
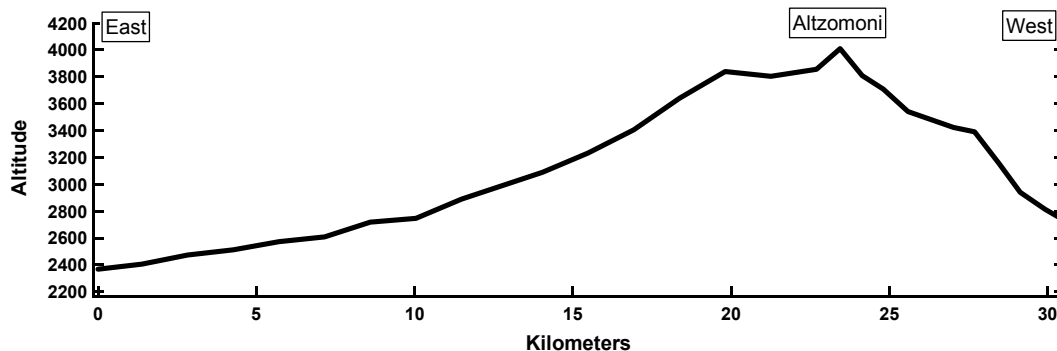
Fig. 5. This diagram is a vertical profile of the topography and shows that the terrain slopes more gradually to the east than to the west from the Altzomoni measurement site. This figure is not to scale.

Fig. 6. These two photographs, taken by the web camera that recorded images every five minutes from the measurement site, show the growth of the regional mixed layer, looking west to the southern edge of Mexico City.
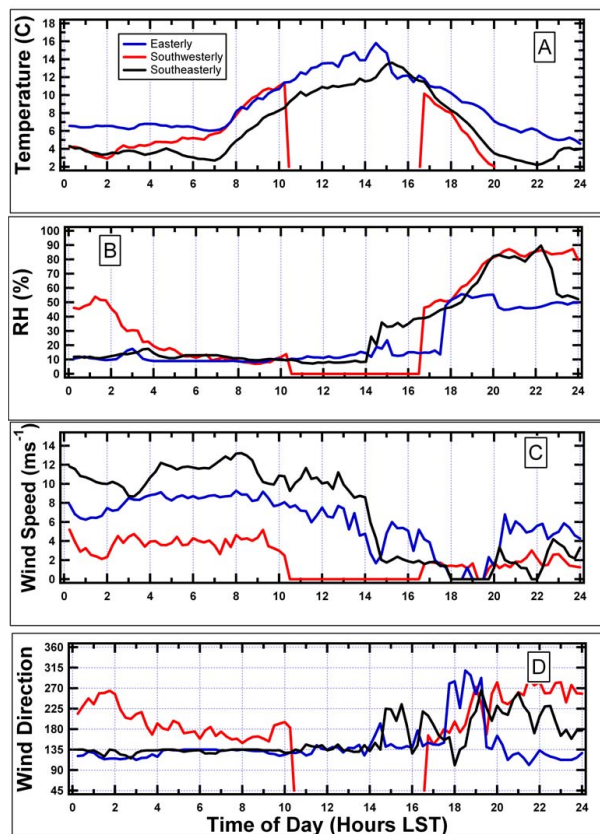
Fig. 7. The diurnal variations in the meteorological patterns of **(A)** temperature, **(B)** relative humidity, **(C)** wind speed and **(D)** wind direction are shown for the three cases of air coming from the east (blue), southwest (red) and southeast (black). Each data point represents a fifteen minute average. There is missing data from 10:00 to 17:00 LST on the day of south-westerly winds due to a weather station malfunction.
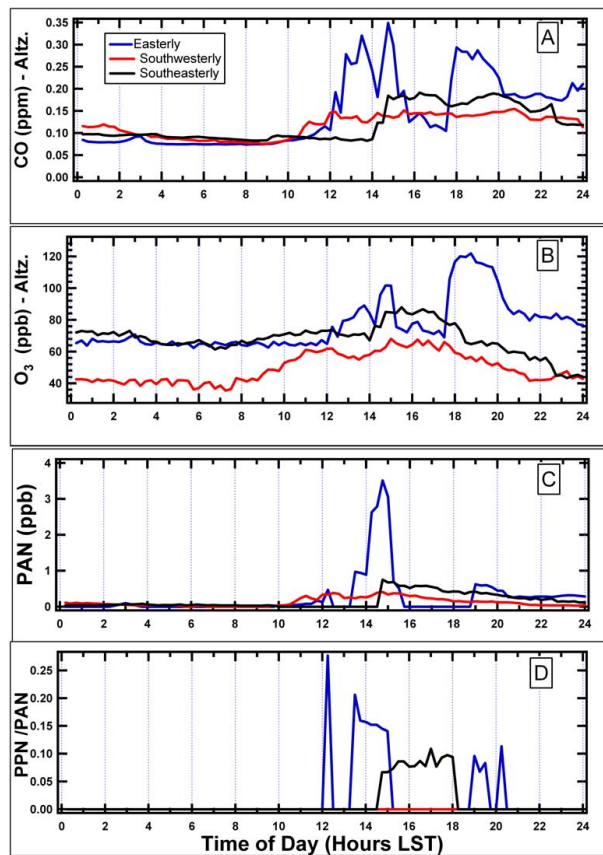
Fig. 8. These time series of **(A)** CO, **(B)** O$_3$, **(C)** PAN and **(D)** the ratio of PPN to PAN are for the same conditions as Fig. 7.
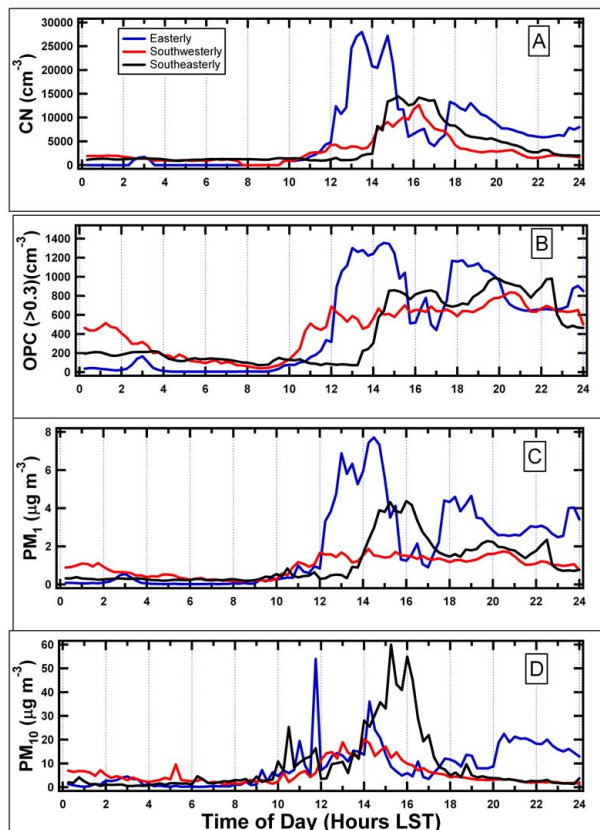
Fig. 9. The diurnal variations in the concentrations of **(A)** condensation nuclei, **(B)** OPC particle >0.3 μm, **(C)** PM$_{1.0}$ and **(D)** PM$_{10}$ are shown for the same conditions as Fig. 7. Note that all concentrations are normalized to standard temperature and pressure.
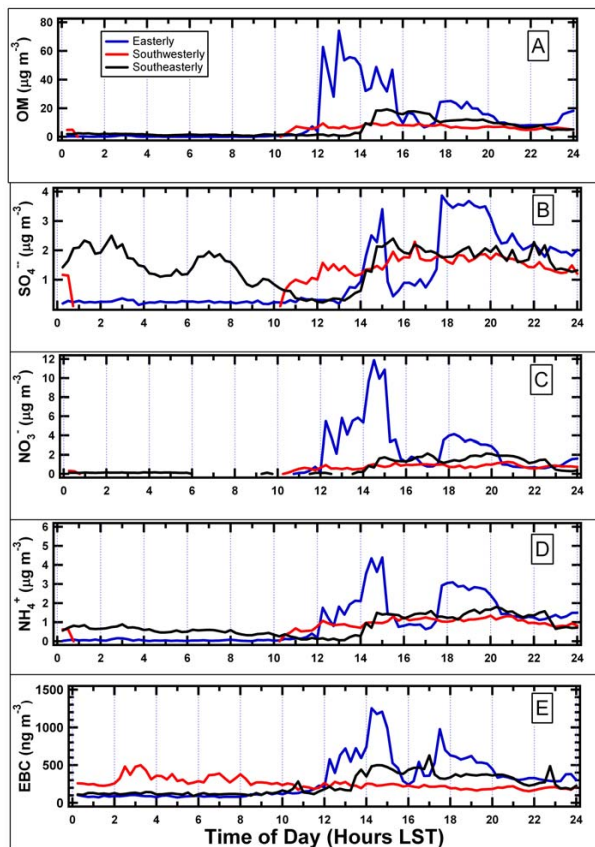
Fig. 10. These time series of ion masses **(A)** organic material, **(B)** sulfate, **(C)** nitrate, **(D)** ammonium measured with the AMS and **(E)** effective black carbon derived from the absorption measurements made with the PSAP, are for the same conditions as Fig. 9. Note that all concentrations are normalized to standard temperature and pressure. There is missing data from the AMS from 01:00 to 10:00 on the day of southwesterly flow due to a power outage.

Full Screen / Esc

Easterly   **Southwesterly**

Night 18:00 – 11:00 LST

Easterly Night: carbox 7%, amine 13%, alkane 11%, alcohol 69%

Southwesterly Night: alcohol 13%, carbox 30%, amine 13%, alkane 45%

Day 11:00 – 18:00 LST

Easterly Day: carbox 5%, amine 26%, alkane 17%, alcohol 53%

Southwesterly Day: carbox 14%, amine 15%, alkane 17%, alcohol 53%
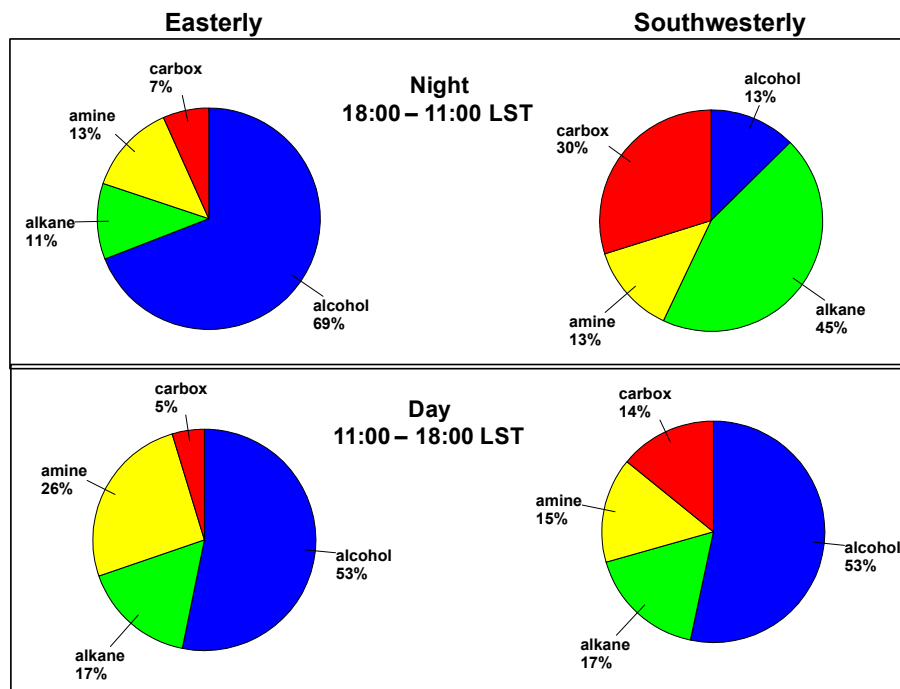
Fig. 11. The FTIR analysis of the components of organic carbon on filters taken in at night (top panel) and during the day (bottom panel) are shown for the cases of flow from the east (left side) and from the southwest (right side). The values are given as percentages of the total organic carbon derived from the analysis.
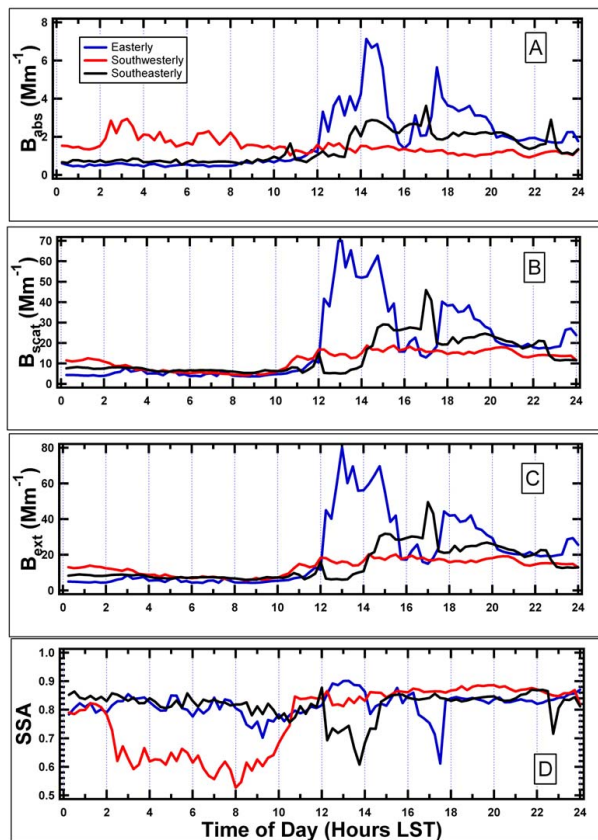
Fig. 12. The optical properties, derived from the nephelometer and PSAP, are shown here in **(A)** absorption coefficient, **(B)** scattering coefficient, **(C)** extinction coefficient and **(D)** single scattering albedo, for the same conditions as Fig. 9.
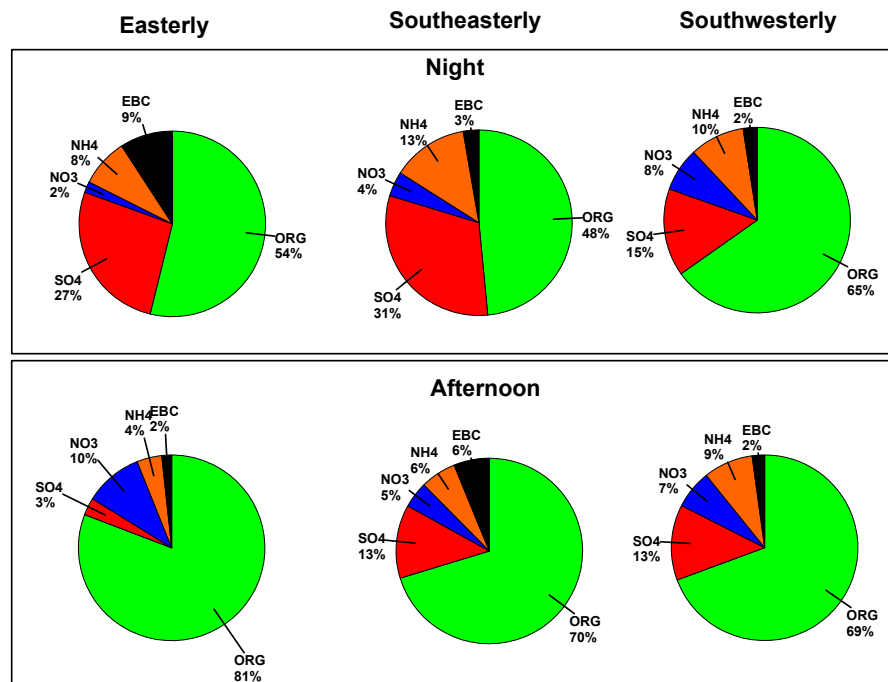
Fig. 13. The mass fraction of ions measured with the AMS and effective black carbon mass derived from the PSAP are shown for the days with flows from the east (left), southeast (center) and southwest (right) for the night time (top panel) and the afternoon (bottom panel).
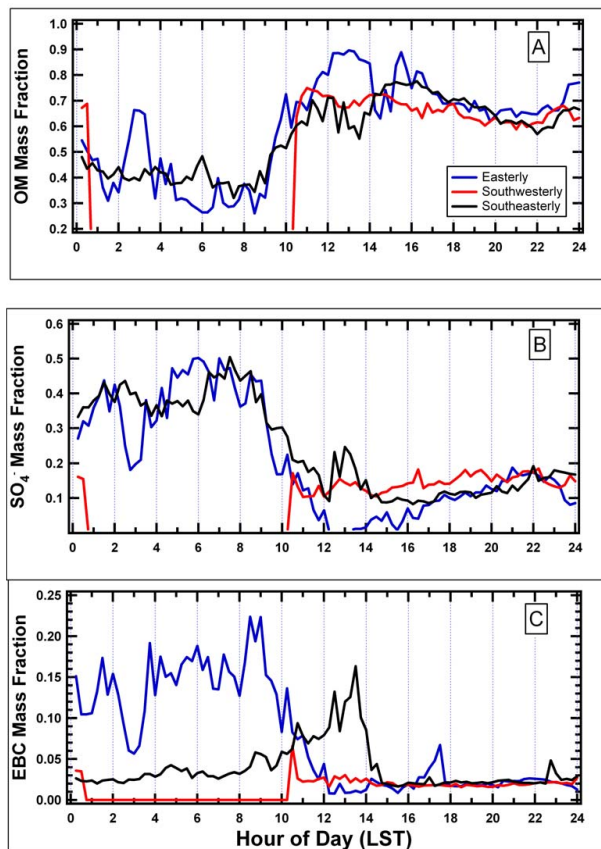
Fig. 14. These diurnal time series are the mass fractions of **(A)** organic material,**(B)** sulfate and **(C)** effective black carbon for the days with different flow directions. Note that the period from 01:00 to 10:00 is missing data due to problems with the AMS during that period.

Title Page

Abstract | Introduction

Conclusions | References

Tables | Figures

◀ | ▶|

◀ | ▶

Back | Close

Full Screen / Esc

Printer-friendly Version
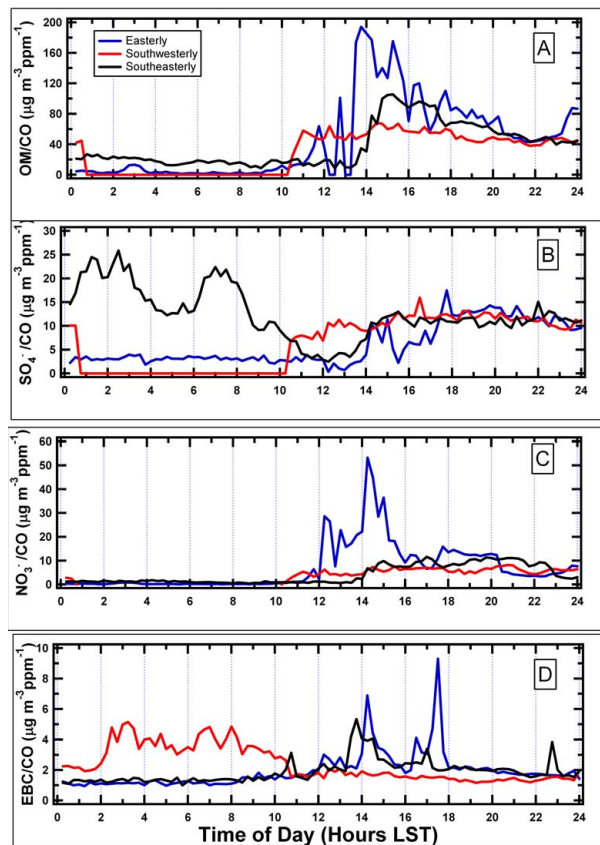
Interactive Discussion

Fig. 15. The AMS ions and EBC have been normalized by the CO to account for air mass dilution, shown here for **(A)** organic material, **(B)** sulfate, **(C)** nitrate and **(D)** effective black carbon.

ACPD

9, 3265–3306, 2009

Pollution in the regional mixed layer of central Mexico

D. Baumgardner et al.

Title Page

Abstract   Introduction

Conclusions   References

Tables   Figures

◀◀   ▶▶

◀   ▶

Back   Close

Full Screen / Esc

Printer-friendly Version
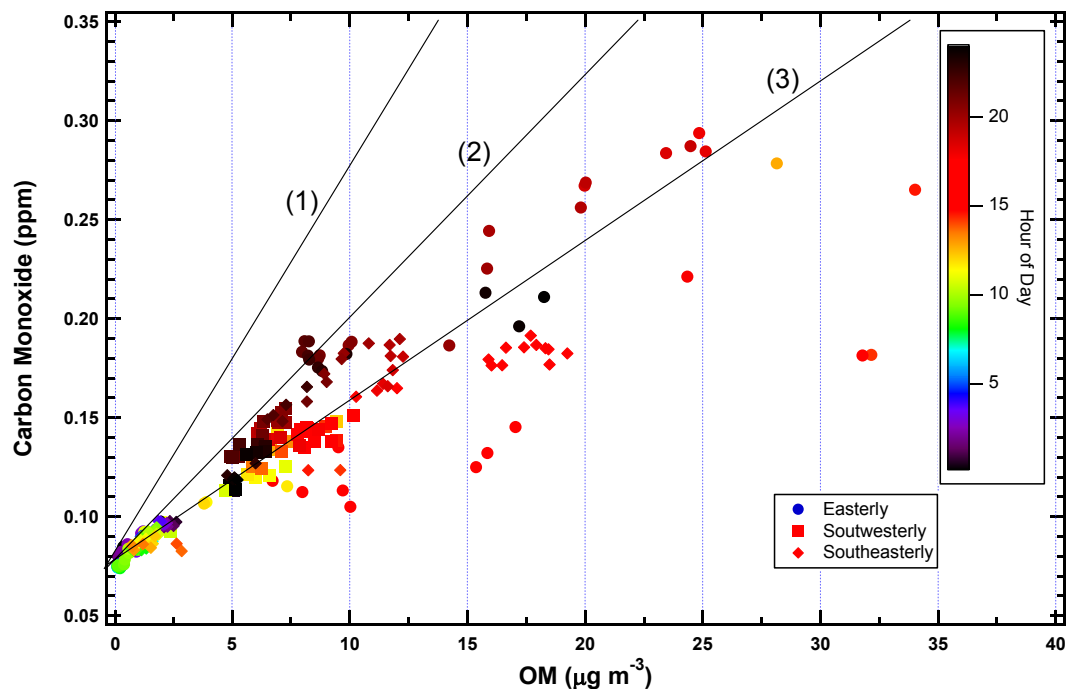
Interactive Discussion

Fig. 16. The carbon monoxide is displayed as a function of organic material measured with the AMS for the days of flow from the east (filled circles), southeast (filled squares) and southwest (filled diamonds). The color of the symbol represents the time of day, shown by the color scale to the right in the figure. The numbered lines correspond to CO/OC slopes from the following emission sources: **(1)** diesel trucks (Lloyd and Cackette, 2001), **(2)** wood burning (Cabada et al., 2002) and **(3)** biomass burning (Andreae and Merlet, 2001).
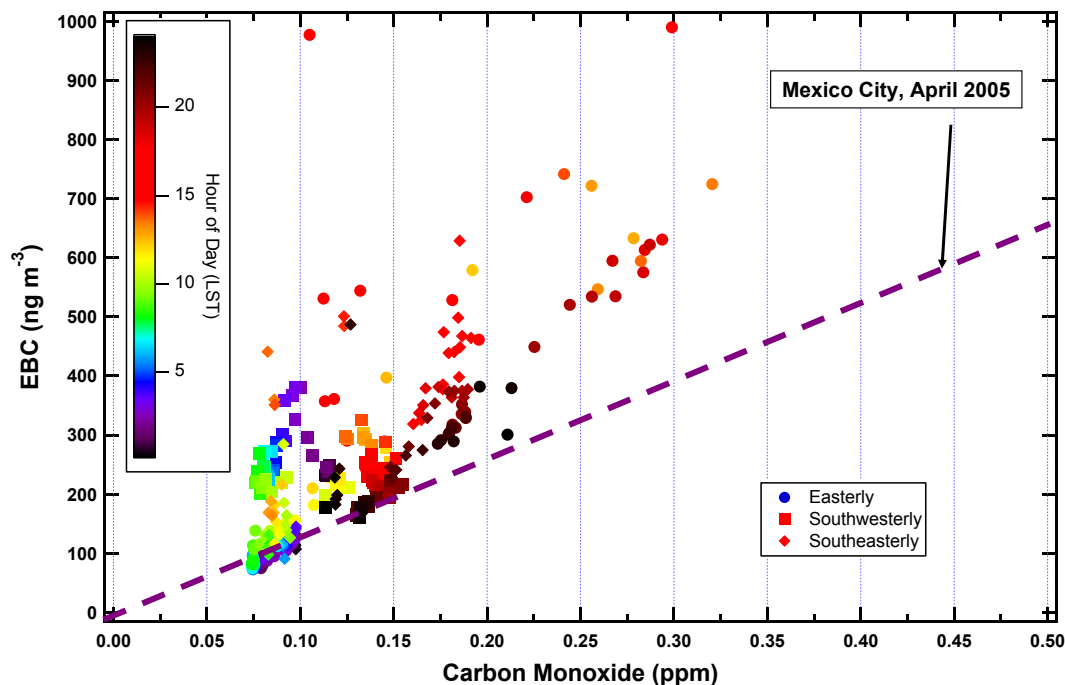
Fig. 17. The effective black carbon is displayed as a function of carbon monoxide for the days of flow from the east (filled circles), southeast (filled squares) and southwest (filled diamonds). The color of the symbol represents the time of day, shown by the color scale to the right in the figure. The dashed line shows the relationship established from measurements made in Mexico City in 2005.

ACPD

9, 3265–3306, 2009

Pollution in the regional mixed layer of central Mexico

D. Baumgardner et al.

Title Page

Abstract | Introduction

Conclusions | References

Tables | Figures

|◄ | ►|

◄ | ►

Back | Close

Full Screen / Esc

Printer-friendly Version

Interactive Discussion